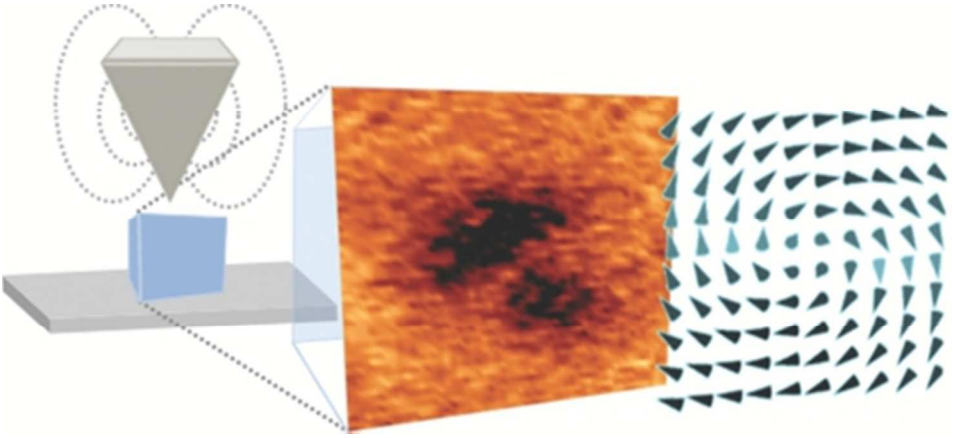

TOC
40x18mm (300 x 300 DPI)

Switching the Magnetic Vortex Core in a Single Nanoparticle

Elena Pinilla-Cienfuegos,[†] Samuel Mañas-Valero, Alicia Forment-Aliaga and Eugenio Coronado**

Instituto de Ciencia Molecular (ICMol). Universitat de València, Catedrático José Beltrán 2, E46980 Paterna, Spain.

Corresponding Author

* Prof. Eugenio Coronado. E-mail: eugenio.coronado@uv.es

* Dr. Alicia Forment-Aliaga. E-mail: alicia.forment@uv.es

ABSTRACT: Imaging and manipulating the spin structure of nano- and mesoscale magnetic systems is a challenging topic in magnetism yielding a wide range of spin phenomena as skyrmions, hedgehog-like spin structures or vortices. A key example has been provided by the vortex spin texture, which can be addressed in four independent states of magnetization, enabling the development of multibit magnetic storage media. Most of the works devoted to the study of the magnetization reversal mechanisms of the magnetic vortices have been focused on micron-size magnetic platelets. Here we report the experimental observation of the vortex state formation and annihilation in individual 25 nm molecular-based magnetic nanoparticles measured by low-temperature variable-field magnetic force microscopy (LT-MFM).

Interestingly, in these nanoparticles the switching of the vortex core can be induced with very small values of the applied static magnetic field.

KEYWORDS: Magnetic Vortices, Nanoparticles, Magnetic Force Microscopy, Magnetization Switching, Low Temperature

Vortices and antivortices are well-known dynamic physical structures comprising phenomena as diverse as the tornadoes formed in the atmosphere, or the quantum vortices found in superconductors and superfluids. In magnetism, a vortex is defined as an in-plane closed-flux magnetization that is characterized by its rotation, clockwise or counter-clockwise ($c = \pm 1$), and by a nanometric-size central spot called vortex core with an out-of-plane magnetization, which can be pointing up or down ($p = \pm 1$).[1-4] These spin textures have been mainly observed and manipulated in quasi-2D micrometric and sub-micrometric objects such as lithographed patterns [1,5] or growth islands [2,6] of ferromagnetic metals and alloys. As a step forward, few examples have been reported for much smaller objects like single magnetic nanoparticles (MNPs), where the vortex has been imaged in the remanent state.[7,8] Magnetic vortices offer great potential as a novel concept in non-volatile data storage devices and other spintronic applications.[9-11] However, the use of MNPs for these purposes requires, not only the stabilization of the magnetic vortex state, but also the active control of the formation and switching of the vortex core.

For the imaging of magnetic vortex cores within MNPs two strict conditions must be accomplished: First, the size of the MNP has to be slightly above the critical single-domain size to form the vortex state[12-14] and, second, a very high resolution imaging technique is needed to be

able to resolve the magnetic configuration inside a single nanometric particle.[2,7] In this scenario, we propose the following approach to satisfy both conditions: First, the use of molecular-based MNPs whose composition, shape and size can be chemically designed to tune the magnetic properties. The chosen systems are magnetically soft nanoparticles of formula $K_{0.22}Ni[Cr(CN)_6]_{0.74}$, from the Prussian blue analogues family.[15,16] They are cubic nanoparticles dispersed in water and can be deposited by simple drop casting on a silicon substrate. Second, the use of the magnetic force microscopy (MFM) working at low-noise conditions (low-temperature (LT) and pressure). In these circumstances, a strong enhancement of the resolution and sensitivity of the technique can be achieved. Thus, permitting the detection of very small force gradients even working with commercial tips.[17] As the system is a variable-field LT-MFM, it allows studying the vortex formation by imaging the magnetic state inside the nanoparticle at different values of the external applied field (B_{ext}).

The spin structure and the magnetization reversal mechanisms of cubic MNPs with sizes around the single-domain critical size have been deeply described by micromagnetic simulations.[18,19] Below the single-domain limit (l_{SD}) different situations can be found. For the smallest MNPs, the uniformly magnetized state prevails conforming the single-domain or flower state, that carries only little anisotropy energy (Figure 1a, cases i and ii). In this case, the magnetization reversal takes place by coherent rotation, so they are below the coherent rotation limit (l_{coh}).[20] By increasing the nanoparticle size, inhomogeneous states become energetically favorable and a twisted flower state, also known as curling state, appears (Figure 1a, case iii). In this region, more complex reversal mechanisms start to appear provoking non-coherent rotation in such a way that the magnetization reversal occurs through a curling process along the easy magnetic axis.[21] For larger sizes slightly above the l_{SD}, the magnetic configuration that becomes

more energetically favored for low anisotropic materials is the so-called vortex state (Figure 1a, case iv). The vortex state presents closed-flux lines inside the MNP and, by definition, the vortex axis would be pointing along the vortex core and perpendicular to the easy axis of the MNP (Figure 1b). In this case, the magnetization reversal takes place *via* vortex formation and annihilation.[14] For larger MNPs ($l >> l_{SD}$), the magnetization reversal will take place *via* domain nucleation and growth, which is the most common switching mechanism in ferromagnetic materials. However, as the MNPs can have real-structure defects at the core or at the surface, it can also induce inhomogeneous reversal mechanisms as localized nucleation or domain wall pinning.[22]

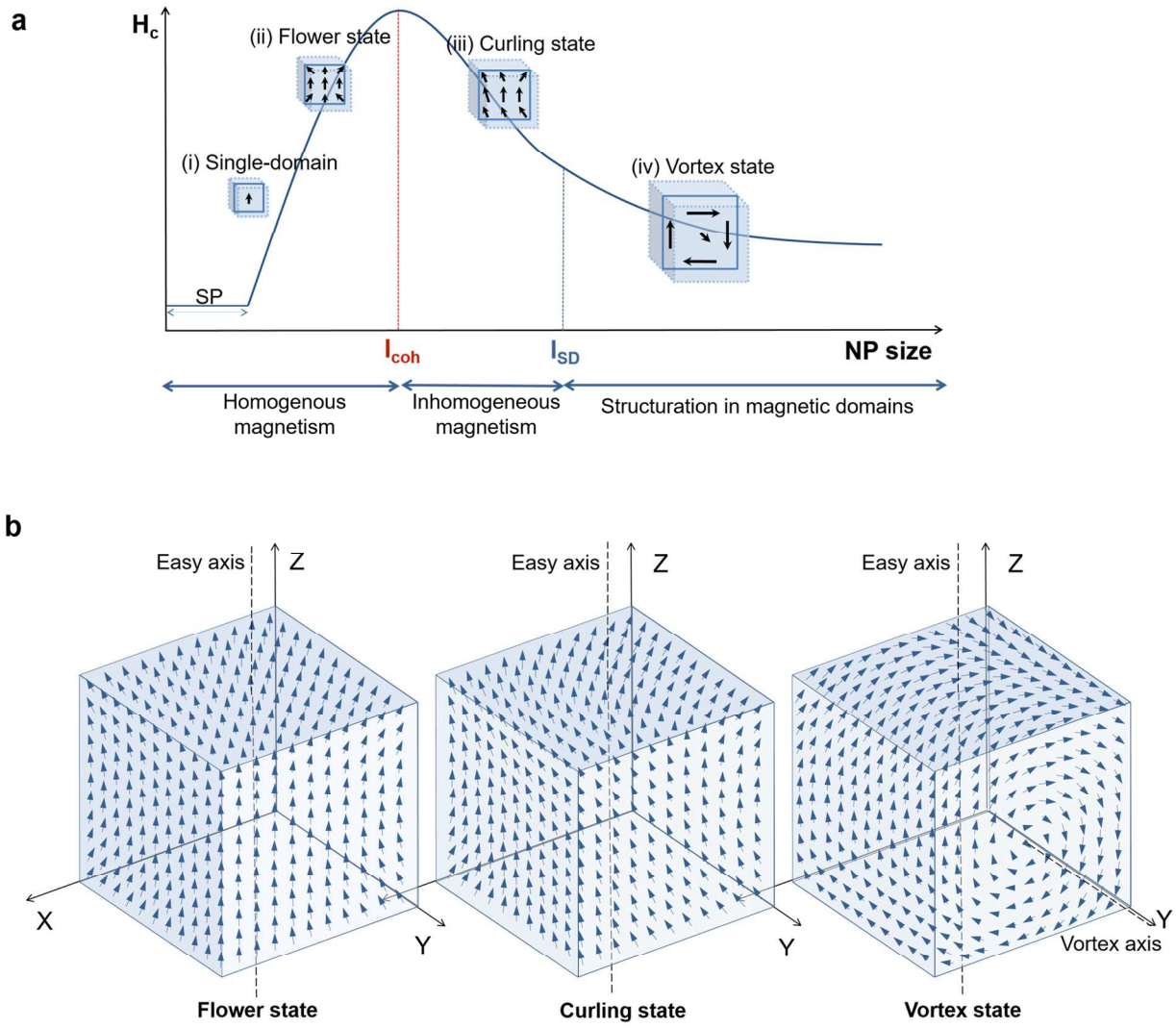

Figure 1. (a) Sketch of the dependence of the magnetization hysteresis loop coercive field (H_c) with the MNP size. Insets: the most energetically favored states of cubic nanoparticles with uniaxial anisotropy. (b) 3D representation of three types of magnetization predicted in a cubic MNP: flower sate, curling state and vortex state.

The chosen MNPs $K_{0.22}Ni[Cr(CN)_6]_{0.74}$ exhibit a Curie temperature (T_C) below 40 K and are almost perfect cubic particles with an aspect ratio between 1 and 1.1 confirmed by transmission electron microscopy.[17] This slight elongation induces shape anisotropy, so the easy axis of magnetization would lie on the long axis of elongation and the hard axes would be along the two

directions perpendicular to the easy axis. Therefore, we can consider these MNPs as cubic particles with a low uniaxial anisotropy and an effective magnetic moment (μ_{NP}), whose orientation can be imaged through MFM. Their average size of 25 nm[23] is above the predicted single-domain regime (around 22 nm) that has been recently estimated by Prado and co-workers for very similar $CsNi[Cr(CN)_6]$ NPs, through the relation between the critical size and the exchange length proposed by Rave *et al.* for cubic MNPs through micromagnetic calculation.[24] Below T_C, μ_{NP} can be frozen and driven by an external magnetic field.[25] All the MFM measurements presented in this work were performed at 4.2 K and at low pressure allowing us to acquire snapshots at every step of the reversal process with the best signal to noise ratio, thus reaching high spatial resolution.

RESULTS AND DISCUSSION

The inspected sample is a group of dispersed MNPs of heights comprised between ~13 nm and ~25 nm in a scanned area of 520 nm x 520 nm, and will present a random distribution on their easy magnetization directions (Figure 2b). The observed behavior of every MNP during the magnetization reversibility process will depend on the orientation of the nanoparticle easy axis, on the MNP size (which determines the intrinsic magnetization of each MNP) and the dipolar interactions. All these factors, together with a study of the hysteretic behavior of these MNPs were previously studied in detail and discussed by us in a previous work.[17] Finally, it is important to highlight that the total magnetic field applied to each MNP is the sum of B_{ext} plus the stray field of the tip (estimated to be in between 370 Oe and 570 Oe, see S.I 1). In the present configuration, with the tip aligned in the +z direction, the dark contrast means an attractive tip-sample interaction so the μ_{NP} is oriented with the external applied field in the +z direction, while

the bright contrast means a repulsive tip-sample interaction and the μ_{NP} would be then pointing to the opposite orientation (-z direction) (Figure 2a). When all the MNPs spins are oriented along B_{ext}, the magnetic contrast presents a symmetric and more confined configuration and reaches the maximum intensity. It is important to note that the intensity of the bright signal is always lower than the intensity of the dark one at the same value of B_{ext} (but in opposite orientation). This is due to the influence of the stray field of the tip that cannot be avoided. When B_{ext} is applied in the same orientation than the magnetization of the tip, both fields are added giving rise to a total field higher than B_{ext}. However, when B_{ext} points to the opposite orientation, there will be a decrease in the resulting field acting over the MNP.

Four cases (nanoparticles labeled in Figure 2b) will be studied in detail: NP1, NP2, NP3 and NP4 with 18 nm, 20 nm, 23 nm and 25 nm sizes, all of them around the predicted $l_{SD} \approx 22$ nm. To start the experiment a static out-of-plane external field (B_{ext}) of +10,000 Oe was applied, so both tip and sample were strongly magnetized and aligned in the +z direction. Then, B_{ext} was varied from -600 Oe to +300 Oe in consecutive steps of 50 Oe. High resolution magnetic images were recorded at every value of the field that allowed for closely follow the magnetic configuration inside each individual MNP (Figure 2c).

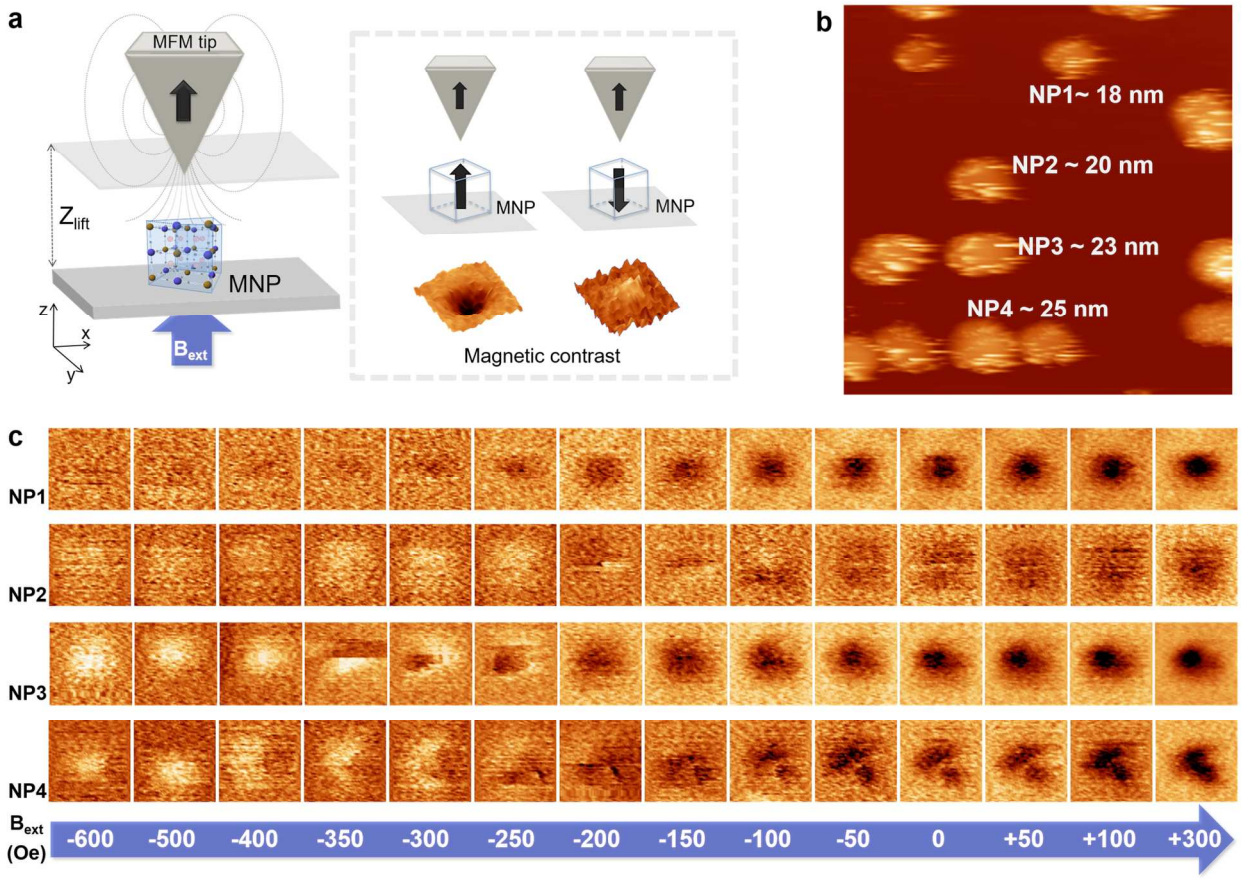

Figure 2. (a) Scheme of the tip-sample relative position and the magnetic contrast formation in MFM. In the configuration with the tip aligned in the +z direction, the dark contrast means an attractive tip-sample interaction so the μ_{NP} is oriented with the external applied field in the +z direction, while the bright contrast means a repulsive tip-sample interaction and the μ_{NP} would be then pointing to the opposite orientation (-z direction). (b) Topographic image of the selected area. The studied MNPs are labeled with number and nanoparticle size. Scan area: 520 nm x 520 nm. (c) Sequence of high resolution magnetic images of the MNPs labeled in (b) at different values of B_{ext}. Scan areas of 115 nm x 115 nm.

The magnetic images for the smallest nanoparticle, NP1~ 18 nm, are shown in the Figure 2c at different values of B_{ext}. At B_{ext} = -600 Oe the image does not show bright contrast. The tip-

sample interaction (the measured MFM contrast) depends on the relative orientation of the magnetization of the tip and the MNP. As already mentioned, if both are opposite and the sum of the spins of the MNP (the effective magnetic moment, μ_{NP}) is not completely reversed, the interaction is weaker, making it very difficult to detect. The absence of a clear bright contrast could indicate that a value of -600 Oe is not sufficient to provoke the complete magnetization reversal of this MNP. Then, B_{ext} is gradually reduced and at -350 Oe, a smoothed dark contrast starts to appear meaning that the μ_{NP} is reversing following the B_{ext}. The μ_{NP} is gradually aligned with B_{ext} while it is swept from -350 Oe to +100 Oe without jumps or discontinuities. Finally, at +300 Oe, a more intense and confined dark area is shown in the magnetic image, so μ_{NP} is fully rotated and aligned with B_{ext}. It is known that the coherent rotation of the spins is accompanied by a substantial increase of the switching field compared to the incoherent switching mechanism.[26] On the other hand, Stoner-Wohlfarth theory predicts that the energy to rotate a single domain MNP would be higher if B_{ext} is aligned with the easy axis of the MNP, and this could be the case of NP1. These two facts would explain why the magnetization reversal of NP1 was not completed. The partial homogeneous magnetization reversibility observed by MFM points out that this is an example of single-domain MNP and the reversal mechanism takes place *via* coherent rotation (Switching process shown in Supporting Information, Video 1).

The second nanoparticle, NP2 ~ 20 nm (Figure 2c) is slightly smaller than the predicted single-domain limit (22 nm). At -600 Oe the magnetic image shows a bright contrast meaning that the μ_{NP} points down (attractive interaction), following the B_{ext}. The bright contrast intensity gradually decreases as B_{ext} is varied from -600 Oe to -250 Oe. This means that the μ_{NP} is following the applied field. Then, the magnetic switching of NP2 can be observed from -200 Oe to -100 Oe, where the magnetic images present a dipolar contrast (dark/bright) evolving with B_{ext}

in the XY plane of the MNP. Finally, the nanoparticle is switched at -50 Oe, showing a smooth dark contrast. The dark contrast of NP2 becomes more intense as the B_{ext} increases and at last, at +300 Oe, the NP is fully switched and saturated. This case corresponds then to a single domain MNP below the single domain limit, and the magnetization reversal takes place *via* non-homogeneous rotation. A possible explanation for this magnetization reversal could be *via* curling, were the twist of the magnetization presents a chiral symmetry that evolves with B_{ext} and finally rotates completely tending to reduce the stray field energy by forming a structure similar to a vortex[14] (the rotation of the magnetization of NP2 is shown in the Supporting Information, Video 2). The magnetic reversal *via* quasi-coherent (curling) of a cubic nanoparticle was simulated by Krone *et al.* some years ago, matching with our experimental data.[19]

The magnetic reversal of the next nanoparticle, NP3 ~ 23 nm, is shown in Figure 2c. At -600 Oe, the μ_{NP} is pointing down (-z direction) showing an overall bright contrast. The bright contrast decreases slightly from -600 Oe to -350 Oe, meaning that the μ_{NP} is rotating by the effect of the B_{ext}. At -350 Oe, a discontinuity is shown as a dark region crossing the MNP. This can be explained if a defect is positioned on the surface of the MNP and the tip strongly interacts with it. At -300 Oe, an activation volume has appeared as a localized area with reversed magnetization (a squared dark region that means that the spins have rotated to an orientation opposite to the initial state). This is consistent with a defect that starts to reverse *via* localized nucleation. Then, the magnetization reversal evolves *via* domain-wall propagation that can be seen in the consecutive magnetic images from -300 Oe to -250 Oe. The reversed region becomes larger until -200 Oe, when the domain pointing down (bright contrast) is completely annihilated. From -200 Oe, only remains one domain with an out-of-plane component (dark contrast) that successively rotates trying to align with the B_{ext} while increasing it. Finally, the magnetic image

at +300 Oe shows an irregular shape of the dark magnetic contrast that could be explained if the easy axis of the μ_{NP} is not completely aligned with the external field (the rotation of the magnetization of NP3 is shown in the Supporting Information, Video 3). In this case, the magnetization reversal was initiated in a small nucleation volume (localized nucleation) around a surface defect that is a source of strong local demagnetizing fields and can act as a nucleation center. The localized nucleation is then produced when the magnetization reversal starts from a very small activation volume at a certain value of the field (switching field) which has reversed its magnetization while the rest of the particle remains at the initial state. This small reversed area propagates when the external field is increased until the whole MNP is reversed completely.

Finally, for the NP4 (~ 25 nm), the initial state is at B_{ext} = -600 Oe where the nanoparticle presents bright contrast meaning that μ_{NP} is pointing down. The μ_{NP} then starts to rotate as B_{ext} is decreased (from -350 Oe to -250 Oe) and two regions (dark/bright) are distinguished. The magnetic configuration of the nanoparticle, therefore the magnetic contrast, is modified as the strength of B_{ext} is decreased and at -250 Oe one domain-wall (DW) with dark contrast appears (Figure 3a, pointed by a yellow arrow). In the next step, two DWs are resolved at -200 Oe (Figure 3a, two centered dark lines in the magnetic image forming a 120° angle pointed by yellow arrows). As the B_{ext} decreases, the DWs collapse into the vortex state and at -100 Oe, the magnetic image resolves a complete vortex structure showing the in-plane circulation (dark/bright regions). At -50 Oe, the magnetic image represents the in-plane magnetization and at the center of this image the vortex core is clearly observed as an out-of-plane bright central dot. At this point, the LT-MFM image reveals the typical dark/bright poles vortex symmetry similar to the ones found by Mironov *et al.* in cobalt nanoparticles that corresponds to quadrupole magnetic moment of magnetization distribution. Following this work, from the

orientation of the in-plane dark/bright regions we can infer that the vortex chirality is clockwise (c = +1).[27] From the bright contrast obtained at the central spot (vortex core) we can also deduce that the vortex core polarization is p = -1.

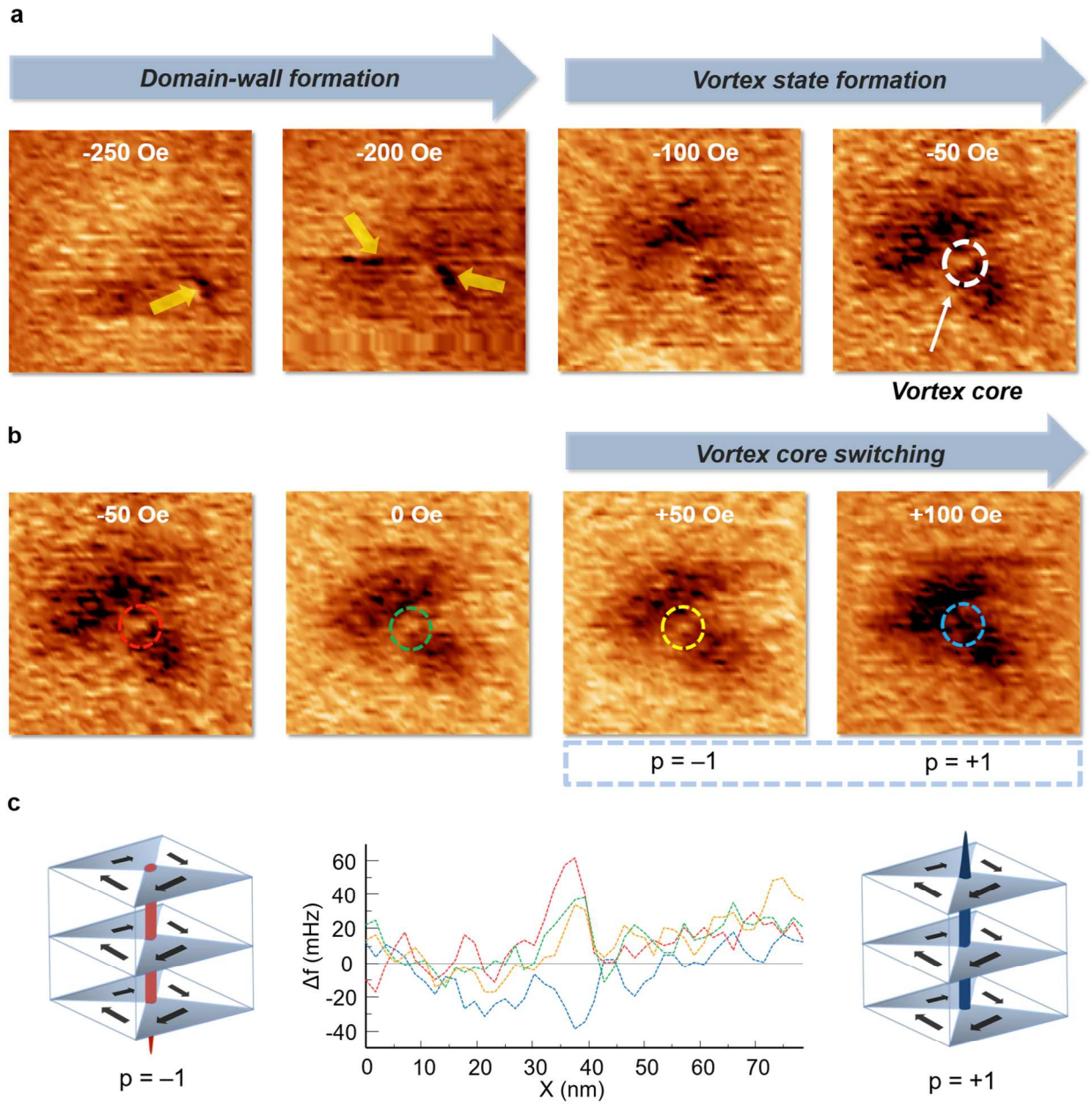

Figure 3. (a) The formation of the DWs is pointed by arrows: at B_{ext} = -250 Oe one DW and at -200 Oe, two DWs are imaged forming a 120° angle. At -150 Oe the magnetic image resolves the

vortex state. At -100 Oe, the magnetic vortex is completely formed with its core pointing down (bright spot highlighted with a white circle). (b) Magnetic images of the vortex core reversal showing how its polarization switches from down (p = -1) to up (p = +1) when B_{ext} changes from +50 Oe to +100 Oe (size of all magnetic images: 115 nm x 115 nm). (c) Sketches of the magnetic vortex with the core pointing down or up, depending on the polarization. The gradual change in the core polarization is shown in the plot of frequency shift profiles of images in (b), as a function of the distance (x-axis tip scan) at different values of B_{ext}. Scan areas of 115 nm x 115 nm.

As can be seen in Figure 3b, the orientation of the nanometric core fully switches from a down state (p = -1) to an up state (p = +1) when B_{ext} changes from +50 Oe to +100 Oe. By increasing B_{ext}, the contrast of the core is gradually reduced and at +100 Oe the vortex core is fully reversed presenting dark contrast. Experimental evidence of the switching of the vortex core from the turn-down magnetization to the turn-up magnetization is shown in Figure 3c where the change of the frequency shift (tip-sample interaction at the vortex core) was plotted as a function of the distance: line profiles were performed crossing the center of each vortex core at each LT-MFM image for different values of B_{ext}. It can be seen that the frequency shift gradually decreases with the decrease of the B_{ext} (from 60 mHz for B_{ext} = -50 Oe, to 38 mHz for B_{ext} = 0 Oe, and finally to 30 mHz for B_{ext} = +50 Oe), showing that the turn-down magnetization of the vortex core is diminished as the external field does. At B_{ext} = +100 Oe, the frequency shift presents a negative value (-40 mHz) indicating that the vortex core was switched. In contrast to the work performed by Wachowiak *et al.* with the spin-polarized scanning tunneling microscope (SP-STM),[2] the real size of the vortex core cannot be estimated from the contrast observed in the LT-MFM images due to tip-convolution effects produced by the MFM tip.[28]

Finally, for higher B_{ext} values the vortex state is annihilated due to the saturation of the magnetization of the MNP. The magnetic images reveal that this MNP has the vortex axis pointing in z-direction. Therefore, the MNP easy axis would point in the XY plane and we can also infer that the magnetization reversal takes place *via* vortex formation and annihilation (the whole switching process of the vortex state can be seen in Supporting Information, Video 4). By taking into account the stray field of the tip (See S.I. 1), we estimate that the reversal of the vortex core takes place at a total applied field of about ~ 470 – 670 Oe.

The observation of a reversal in the vortex core polarity by an out of plane B_{ext} as small as few hundreds Oe is quite remarkable, as this field is one order of magnitude smaller than those required to invert the vortex core polarity in circular micrometric dots.[28,29] Besides the differences in size between the circular micrometric dots and our MNPs, there are also important differences in the shapes of the magnetic structures that could be the origin of this observation. The quasi-2D magnetic structures, exhibit an in-plane magnetization in order to reduce the magnetostatic energy characteristic of thin films of soft magnetic materials with lateral size larger than the magnetic exchange length.[1,30] The reversal of the vortex core for flat ferromagnetic structures is a process driven by the exchange field, so samples with a higher aspect ratio (diameter/thickness) require larger switching fields. This is the reason why a flatter sample has a larger demagnetizing factor in the perpendicular direction.[31] In the case of cubic ferromagnetic NPs with uniaxial anisotropy, the switching field depends on the sample size (with all other material parameters kept fixed). Therefore, there is a suitable size where the vortex state appears as the ground state. In the present case, the vortex state appears in a nanoparticle as small as 25 nm, near the estimated critical single-domain limit of 22 nm. In consequence, this

small size requires a significant low value of the static switching field to reverse the MNP vortex core.

Finally, we have observed magnetic vortices in other MNPs with similar sizes supporting the robustness of the formation of the vortex state in this type of nanoparticles. A MNP of 23 nm height (and more elongated than the preceding particles) was inspected. A complete study of the magnetization reversal of this MNP was achieved by sweeping the B_{ext}, from negative to positive field (from -600 Oe to +600 Oe) and from positive to negative field (from +600 Oe to -600 Oe) as can be seen in the Figure S2a. In this case, as happened in the NP4, at the first stages of the magnetization reversal the DWs formation is imaged (from -600 Oe to -500 Oe). At -400 Oe, the closed-flux in-plane magnetization of the vortex state is observed, thus, the magnetic vortex core is located at the DWs junctions.[32] The annihilation of the vortex state, and therefore the complete magnetization reversal of this MNP was achieved at -150 Oe where an overall dark contrast is shown in the magnetic image. A clearer example of the DWs propagation and annihilation is shown in the Figure S2b, where the magnetization reversal of a MNP of 28 nm height (with parallelepiped shape) was imaged. In this case the asymmetry of the magnetic configuration could correspond to an asymmetric vortex state due to the elongated shape of the nanoparticle or due to a vortex core located at the corner of nanoparticle.[13,32]

CONCLUSIONS

In summary, by varying the size of the MNP various cases of magnetization reversal mechanisms in MNPs have been observed: coherent rotation, non-coherent rotation (curling and localized nucleation) and finally *via* vortex formation and annihilation, within single and isolated particles. In particular, the vortex spin texture, including its vortex core, has been experimentally

observed and manipulated in a single MNP (25 nm) conveniently designed to be above the critical single-domain size. We have demonstrated that the reversal in the polarization of the vortex core in these chemically-designed nanoparticles can be induced with an unprecedented small value of the perpendicular static magnetic field.

Overall, our finding opens the possibility of using the polarization of the vortex core of individual MNPs prepared by chemical methods as bits of memory of nanometric size, which can be manipulated with much smaller external fields than those required in flat micrometric magnetic dots prepared by lithographic methods.

The results reported here have been performed at 4 K. Such a small value is not imposed by the low Curie temperature of these molecular-based nanoparticles (T_C < 40 K), but rather by the ability to reach high resolution MFM images, which will be impossible to obtain working in the conditions reported for micrometric magnetic dots (room temperature and ambient pressure). In fact, at 4 K we are already at the limit for observing through MFM the vortex core in MNPs of such a small size. In any case, our results can be extrapolated to inorganic magnetic nanoparticles having higher T_C values (even above room temperature). Recently, some other magnetic spin textures as skyrmions have been suggested as a bit operation for information storage since they show fascinating properties and can be of nanometric dimensions, similar to the vortex state presents in our MNPs.[33-35] Even for skyrmionics systems, which are observed in layers of materials with high T_C values, the characterization measurements are performed at low temperature to enhance sensitivity. Thus, temperature is not the only factor to take into account for the applicability of MNPs as bits of memory of nanometric size.

MATERIALS AND METHODS

***LT-MFM measurements**:* The commercial LT-MFM (Attocube) operates at very low pressure with a commercial magnetic-coated cantilever (MFMR Nanosensors, 75 KHz resonance frequency and 3 N/m cantilever constant). The instrument has a RMS noise around 2 mHz (the noise limit is 0.78 pm·$Hz^{-1/2}$). The behavior of the used tip under an external out-of-plane applied field at 4.2 K was previously analyzed and a coercive field of ±750 Oe was found. Although the height of isolated nanoparticles can be accurately characterized with the tip of the MFM, the apparent lateral dimensions of the NPs whose size are comparable or even smaller than the tip radius curvature, are substantially increased by the well-known tip-sample convolution effect.[36] Previously any magnetic characterization, the sample was scanned in dynamic mode to acquire the topography and compensate the tilt. Due to the size tip-radius of the magnetic-coated tip ($r \approx 50$ nm) it is not possible to resolve the cubic shape of the $K_{0.22}Ni[Cr(CN)_6]_{0.74}$ MNPs. To record the MFM data we work in *Constant-height Mode* where the sample is retracted at a constant distance (Z_{lift}) from the tip selected to be 100 nm, in order to prevent as much as possible the effect of the stray field from the tip apex. At this distance, the tip scans a plane over the sample obtaining a magnetic map of the scanned area given by the frequency shift (Δf) caused by the magnetostatic tip-sample interactions. Because of these magnetostatic tip-sample interactions, the free resonant frequency of the cantilever f_0 is shifted by Δf, where $\Delta f = f - f_0$. In our case, a Phase Locked Loop (PLL) is used to "track" the frequency shift. The PLL feedback parameters have to be set for every measurement and are extremely sensitive to the environment conditions. A negative frequency shift indicates an attractive tip-sample interaction ($\Delta f < 0$, dark contrast) while a positive frequency shift indicates a repulsive tip-sample interaction ($\Delta f > 0$, bright contrast).

For all the cases, the B_{ext} was changed at a rate of 0.606 $Oe \cdot s^{-1}$. All the LT-MFM acquired data were processed with WSxM software.[37]

On a standard topography image (1 μm^2) we can observe around 80 nanoparticles, and approx. 52% are aggregated, so it is not possible to perform a detailed evaluation of their magnetic reversibility process as they are harder to access with the MFM tip and their reversibility can be dominated by inter-particle interactions (these are bare nanoparticles without capping).

Around 21% of the nanoparticles are isolated and smaller than 19 nm, and 60% of them show homogeneous reversibility or a blocked magnetization without reversibility. Finally almost 90% of nanoparticles higher than 19 nm present non-homogeneous magnetization reversibility processes and, in particular, we were able to identify the vortex state in one third of them.

Synthesis of KNiCr-NPs: $K_{0.22}Ni[Cr(CN)_6]_{0.74}$ NPs were prepared following the synthetic procedure developed for the stabilization of bare $Cs_{0.7}Ni[Cr(CN)_6]_{0.9}$ NPs described in reference 38. The same procedure without the addition of the cesium salt gives rise to the stabilization of bare $K_{0.22}Ni[Cr(CN)_6]_{0.74}$.

AUTHOR INFORMATION

Present Addresses

† Centro de Tecnología Nanofotónica de Valencia (NTC). Universidad Politécnica de Valencia. Camino de Vera s/n. E46022 Valencia, Spain.

Author Contributions

The manuscript was written through contributions of all authors. All authors have given approval to the final version of the manuscript.

Funding Sources

Financial support was provided by the EU (ERC Advanced Grant SPINMOL), the Spanish MINECO (MAT2014-56143-R co-financed by FEDER and Excellence Unit "María de Maeztu" MDM-2015-0538), and the Generalidad Valenciana (Programs Prometeo and ISIC-NANO).

ACKNOWLEDGMENTS

We thank L. Catala, T. Mallah, A. Asenjo and M. Jaafar, for helpful discussions and A. López-Muñoz and E. Tormos for their technical support. We acknowledge the financial support from the Spanish MINECO (MAT2014-56143-R co-financed by FEDER and Excellence Unit "María de Maeztu" MDM-2015-0538), the EU (ERC Advanced Grant SPINMOL) and the Generalidad Valenciana (Programs Prometeo and ISIC-NANO). E.C. thanks the French MENESR and the île de France region for a Blaise Pascal Chair. S.M.-V. and A.F.-A. thanks the Spanish MINECO for the F.P.U. fellowship and R y C grant, respectively.

ASSOCIATED CONTENT

Supporting Information Available: a more detail explanation about methods, MFM images of other examples of magnetic vortices in MNPs and the videos of the magnetization switching of the MNPs. This material is available free of charge *via* the Internet at http://pubs.acs.org.

REFERENCES

(1) Shinjo, T.; Okuno, T.; Hassdorf, R.; Shigeto, K.; Ono, T. Magnetic Vortex Core Observation in Circular Dots of Permalloy. *Science* **2000**, *289*, 930–932.

(2) Wachowiak, A.; Wiebe, J.; Bode, M.; Pietzsch, O.; Morgenstern, M.; Wiesendanger, R. Direct Observation of Internal Spin Structure of Magnetic Vortex Cores. *Science* **2002**, *298*, 577-580.

(3) Van Waeyenberge, B.; Puzic, A.; Stoll, H.; Chou, K. W.; Tyliszczak, T.; Hertel, R.; Fähnle, M.; Brückl, H.; Rott, K.; Reiss, G.; Neudecker, I.; Weiss, D.; Back C. H.; Schütz, G. Magnetic Vortex Core Reversal by Excitation with Short Bursts of an Alternating Field. *Nature* **2006**, 444, 461-464.

(4) Im, M.-Y.; Fischer, P.; Yamada, K.; Sato, T.; Kasai, S.; Nakatani, Y.; Ono, T. Symmetry Breaking in the Formation of Magnetic Vortex States in a Permalloy Nanodisk. *Nat. Commun.* **2012**, *3*, 983.

(5) Choe, S.-B.; Acremann, Y.; Scholl, Y. A.; Bauer, A.; Doran, A.; Stöhr, J.; Padmore, H. A. Vortex Core-Driven Magnetization Dynamics. *Science* **2004**, *304,* 420-422.

(6) Masseboeuf, A.; Fruchart, O.; Toussaint, J. C.; Kritsikis, E.; Buda-Prejbeanu, L.; Cheynis, F.; Bayle-Guillemaud, P.; Marty, A. Dimensionality Crossover in Magnetism: from Domain Walls (2D) to Vortices (1D). *Phys. Rev. Lett.* **2010**, *104*, 127204.

(7) Snoeck, E.; Gatel, C.; Lacroix, L. M.; Blon, T.; Lachaize, S.; Carrey, J.; Respaud, M.; Chaudret, B. Magnetic Configurations of 30 nm Iron Nanocubes Studied by Electron Holography. *Nano Lett.* **2008**, *8*, 4293-4298.

(8) Lacroix, L. M.; Lachaize, S.; Hue, F.; Gatel, C.; Blon, T.; Tan, R. T.; Carrey, J.; Warot-Fonrose, B.; Chaudret, B. Stabilizing Vortices in Interacting Nano-Objects: A Chemical Approach. *Nano Lett.* **2012**, *12*, 3245-3250.

(9) Yamada, K.; Kasai, S.; Nakatani, Y.; Kobayashi, K.; Kohno, H.; Thiaville, A.; Ono, T. Electrical Switching of the Vortex Core in a Magnetic Disk. *Nat. Mater.* **2007**, *6*, 270-273.

(10) Pribiag, V. S.; Krivorotov, I. N.; Fuchs, G. D.; Braganca, P. M.; Ozatay, O.; Sankey, J. C.; Ralph, D. C.; Buhrman, R. A. Magnetic Vortex Oscillator Driven by D.C. Spin-polarized Current. *Nat. Phys.* **2007,** *3*, 498-503.

(11) Ono, T. Magnetic Nanostructures: Vortices on the Move. *Nat. Nanotechnol.* **2014**, *9*, 96-97.

(12) Schabes, M. E.; Bertram, H. N. J. Magnetization Processes in Ferromagnetic Cubes. *Appl. Phys.* **1988**, *64*, 1347-1357.

(13) Rave, W.; Fabian, K.; Hubert, A. J. Magnetic States of Small Cubic Particles with Uniaxial Anisotropy. *J Magn. Magn. Mater.* **1998**, *190*, 332-348.

(14) Hertel, R.; Kronmüller, H. Finite Element Calculations on the Single-Domain Limit of a Ferromagnetic Cube—a Solution to μMAG Standard Problem No. 3. *J. Magn. Magn. Mater.* **2002**, *238*, 185-199.

(15) Gadet, V.; Mallah, T.; Castro, I.; Verdaguer, M.; Veillet, P. High-Tc Molecular-Based Magnets: A Ferromagnetic Bimetallic Chromium(III)-Nickel(II) Cyanide with Tc= 90 K. *J. Am. Chem. Soc.* **1992**, *114*, 9213-9214.

(16) Buser, H. J.; Schwarzenbach, D.; Petter, W.; Ludi, A. The Crystal Structure of Prussian Blue: $Fe_4[Fe(CN)_6]_3 \cdot xH_2O$. *Inorg. Chem.* **1977**, *16*, 2704-2710.

(17) Pinilla-Cienfuegos, E.; Kumar, S.; Mañas-Valero, S.; Canet-Ferrer, J.; Catala, L.; Mallah, T.; Forment-Aliaga, A.; Coronado, E. Imaging the Magnetic Reversal of Isolated and Organized Molecular-based Nanoparticles Using Magnetic Force Microscopy Magnetic Force Microscopy. *Part. Part. Syst. Charact.* **2015**, *32*, 693–700.

(18) McMichael, R. D. Micromagnetic Modeling Activity Group (μMAG). National Institute of Standards and Technology (NIST). http://www.ctcms.nist.gov/~rdm/mumag.html (accessed July 23, 1998).

(19) Krone, D.; Makarov, M.; Albrecht, T.; Schrefl, D. Magnetization Reversal Processes of Single Nanomagnets and their Energy Barrier. *J. Magn. Magn. Mater.* **2010***, 322*, 3771–3776.

(20) Stoner, E. C.; Wohlfarth, E. P. A Mechanism of Magnetic Hysteresis in Heterogeneous Alloys. *Philos. Trans. R. Soc.*, *A* **1948**, *240*, 599-642.

(21) Aharoni, A.; Shtrikman, S. Magnetization Curve of the Infinite Cylinder. Phys. Rev. 1958, *109*, 1522- 1528.

(22) Skomski, R.; Zhou, J. Nanomagnetic Models. In Advanced Magnetic Nanostructures; Springer Science+ Busyness Media: New York, 2006; pp 41-82.

(23) Coronado, E.; Forment-Aliaga, A.; Pinilla-Cienfuegos, E.; Tatay, S.; Catala, L.; Plaza, J. A. Nanopatterning of Anionic Nanoparticles Based on Magnetic Prussian-Blue Analogues. *Adv. Funct. Mater.* **2012**, *22*, 3625–3633.

(24) Prado, Y.; Mazerat, S.; Rivière, E.; Rogez, G.; Gloter, A.; Stéphan, O.; Catala, L.; Mallah, T. Magnetization Reversal in $CsNi^{II}Cr^{III}(CN)_6$ Coordination Nanoparticles: Unravelling Surface Anisotropy and Dipolar Interaction Effects. *Adv. Funct. Mater*. **2014**, *24*, 5402–5411.

(25) Catala, L.; Volatron, F.; Brinzei, D.; Mallah, T. Functional Coordination Nanoparticles. *Inorg. Chem.* **2009***, 48*, 3360–3370.

(26) Frei, E. H.; Shtrikman, S.; Treves, D. Critical Size and Nucleation Field of Ideal Ferromagnetic Particles. *Phys. Rev.* **1957**, *106*, 446-455.

(27) Mironov, V. L.; Gribkov, B. A.; Fraerman, A. A.; Gusev, S. A.; Vdovichev, S. N.; Karetnikova, I. R.; Nefedov, I. M.; Shereshevsky, I. A. MFM Probe Control of Magnetic Vortex Chirality in Elliptical Co Nanoparticles. *J. Magn. Magn. Mater.* **2007***, 312*, 153–157.

(28) Okuno, T.; Shigeto, K.; Ono, T.; Mibu, K.; Shinjo, T. MFM Study of Magnetic Vortex Cores in Circular Permalloy Dots: Behavior in External Field. *J. Magn. Magn. Mater*. **2002**, *240*, 1-6.

(29) Kikuchi, N.; Okamoto, S.; Kitakami, O.; Shimada, Y.; Kim, S. G.; Otani, Y.; Fukamichi, K. Vertical Bistable Switching of Spin Vortex in a Circular Magnetic Dot. *J. Appl. Phys.* **2001**, *90*, 6548-6549.

(30) Coey, J. M. D. Micromagnetism, domains and hysteresis. In Magnetism and magnetic *materials*; Cambridge University Press: Cambridge, 2009; pp. 231-263.

(31) Thiaville, A.; Garcia, J. M.; Dittrich, R.; Milta, J.; Schrefl, T. Micromagnetic Study of Bloch-Point-Mediated Vortex Core Reversal. *Phys. Rev. B* **2003**, *67*, 094410.

(32) Hubert, A. The Role of "Magnetization Swirls" in Soft Magnetic Materials J. Phys. *Colloques*. **1988**, *49*, C8-1859-C8-1864.

(33) Hagemeister, J.; Romming, N; von Bergmann, K.; Vedmedenko, E.Y.; Wiesendanger, R. Stability of Single Skyrmionic Bits. *Nat. Commun.* **2015**, *6*, 8455.

(34) Romming, N; Hanneken, K.; Menzel, M.; Bickel, J. E.; Wolter, B.; von Bergmann, K.; Kubetzka, A.; Wiesendanger, R. Writing and Deleting Single Magnetic Skyrmions *Science* **2013**, *341*, 636-639.

(35) Hanneken, K.; Otte, F.; Dupé, B.; Romming, N.; von Bergmann, K.; Wiesendanger, R.; Heinze S. Electrical Detection of Magnetic Skyrmions by Tunnelling Non-Collinear Magnetoresistance *Nat. Nanotechnol.* **2015**, *10*, 1039–1042.

(36) Canet-Ferrer, J.; Coronado, E.; Forment-Aliaga, A.; Pinilla-Cienfuegos, E. Correction of the Tip Convolution Effects in the Imaging of Nanostructures Studied Through Scanning Force Microscopy. *Nanotechnology* **2014**, *25*, 395703.

(37) Horcas, I.; Fernández, R.; Gómez-Rodríguez, J. M.; Colchero, J.; Gómez-Herrero, J.; Baro, A. M. WSXM: A Software for Scanning Probe Microscopy and a Tool for Nanotechnology. *Rev. Sci. Instrum.* **2007**, *78*, 013705-8.

(38) Brinzei, D.; Catala, L.; Louvain, N.; Rogez, G.; Stéphan, O.; Gloter, A.; Mallah T. Spontaneous Stabilization and Isolation of Dispersible Bimetallic Coordination Nanoparticles of $Cs_xNi[Cr(CN)_6]_y$. *J. Mater. Chem.* **2006**, *16*, 2593-2599.